AIP | Journal of Applied Physics

Mixed structural face-centered cubic and body-centered cubic orders in near stoichiometric Fe2MnGa alloys

Y. V. Kudryavtsev, A. E. Perekos, N. V. Uvarov, M. R. Kolchiba, K. Synoradzki, and J. Dubowik

Citation: Journal of Applied Physics **119**, 205103 (2016); doi: 10.1063/1.4952392
View online: http://dx.doi.org/10.1063/1.4952392
View Table of Contents: http://scitation.aip.org/content/aip/journal/jap/119/20?ver=pdfcov
Published by the AIP Publishing

Articles you may be interested in

Structural and magnetic properties of the Heusler compound Fe2MnGa
J. Appl. Phys. **113**, 17E301 (2013); 10.1063/1.4794979

Influence of site occupancy on the structure, microstructure and magnetic properties of ternary and quasi-ternary alloys of Ni-Mn-Ga
AIP Conf. Proc. **1461**, 74 (2012); 10.1063/1.4736874

Structural and magnetic properties of a chemically ordered face-centered-cubic (111) Mn alloy film
J. Appl. Phys. **99**, 08N504 (2006); 10.1063/1.2163324

Shape memory and ferromagnetic shape memory effects in single-crystal Ni 2 MnGa thin films
J. Appl. Phys. **95**, 2593 (2004); 10.1063/1.1643199

Magnetic properties and martensitic transformation in quaternary Heusler alloy of NiMnFeGa
J. Appl. Phys. **92**, 5006 (2002); 10.1063/1.1511293

Reuse of AIP Publishing content is subject to the terms at: https://publishing.aip.org/authors/rights-and-permissions. Download to IP: 79.191.72.235 On: Sat, 04 Jun 2016 17:02:58

Mixed structural face-centered cubic and body-centered cubic orders in near stoichiometric Fe_2MnGa alloys

Y. V. Kudryavtsev,[1,2] A. E. Perekos,[1] N. V. Uvarov,[1] M. R. Kolchiba,[1] K. Synoradzki,[3] and J. Dubowik[3]
[1]*Institute of Metal Physics, NAS of the Ukraine, Vernadsky 36, 03680 Kiev-142, Ukraine*
[2]*Donetsk Physical and Technical Institute, NAS of the Ukraine, Nauki 46, 03028 Kiev, Ukraine*
[3]*Institute of Molecular Physics, Polish Academy of Sciences, Smoluchowskiego 17, 60-179 Poznań, Poland*

(Received 13 March 2016; accepted 10 May 2016; published online 24 May 2016)

Magnetic and transport properties of near stoichiometric metastable $Fe_xMn_yGa_z$ alloys ($46 \le x \le 52$, $17 \le y \le 25$, $26 \le z \le 30$) with face-centered cubic (FCC), body-centered cubic (BCC), and two-phase (FCC + BCC) structures are investigated. The experimental results are analyzed in terms of first-principles calculations of stoichiometric Fe_2MnGa alloy with the $L2_1$, $L1_2$, and the tetragonally distorted $L2_1$ structural orderings. It is shown that the pure BCC and FCC phases have distinct magnetic and transport properties. Two-phase Fe_2MnGa alloys have magnetic and transport properties typical of the mixed BCC and FCC phases. Among the investigated alloys, $Fe_{46}Mn_{24}Ga_{30}$ has a martensitic transformation accompanied with significant changes of its magnetic and transport properties. *Published by AIP Publishing.* [http://dx.doi.org/10.1063/1.4952392]

INTRODUCTION

Significant interest in stoichiometric and off-stoichiometric Fe_2MnGa Heusler alloys (HAs) has arisen due to the many effects discovered to date: a martensitic transformation,[1–5] a metamagnetic transformation from an antiferromagnetic (AFM) to a ferromagnetic (FM) phase,[6–9] and a large exchange bias.[6–8]

Unlike Ni-Mn-based HA,[10] the Fe_2MnGa alloys can have a more complex magnetic behavior due to the multiple structures in which they may crystallize. For single phase γ-Fe_2MnGa alloys (i.e., alloys with a face-centered cubic (FCC) structure), a FM to AFM transformation has been observed at 220–250 K.[6–9,11] However, as has been found in $Fe_{50}Mn_{24}Ga_{26}$,[9] even a small deviation from stoichiometric composition results in a mixed body-centered cubic (BCC) and FCC structure, with their respective magnetic transformation from a FM to a paramagnetic (PM) state at 190 K and an AFM to FM transformation at 240 K. In this way, the nearly stoichiometric Fe_2MnGa alloys may crystallize either in the BCC or FCC types of structure. Okumura *et al.*[12] have shown that a small change in the melt-spinning processing parameter results in the formation of Fe_2MnGa alloys with BCC or FCC crystal structures from the same precursor ingots. It has been experimentally shown by Yin *et al.*[13] that among the Fe-based HAs, Fe_2MnGa has the minimal negative enthalpy of formation. The stability of the FCC or BCC phases in Fe_2MnGa alloys has been estimated in terms of a valence-electron-to-atom (e/a) ratio that determines the structural transformation by affecting the instability of a phonon mode.[14,15]

On the other hand, a distinct martensitic transformation has also been found in slightly off-stoichiometric Fe_2MnGa alloys. Zhu *et al.*[1] have observed martensitic transformation in $Fe_{50.0}Mn_{22.5}Ga_{27.5}$ alloy from a parent austenite PM BCC phase (with the lattice parameter $a = 0.5856$ nm) to a martensite FM body-centered tetragonal (BCT) structure ($a = b = 0.5328$ nm and $c = 0.7113$ nm). Several publications have reported experimental studies of martensitic transformation in slightly off-stoichiometric Fe_2MnGa alloys having a BCC parent austenite phase.[2–5] The martensite phase has an $L1_0$ (or $D0_{22}$) structure with the lattice parameters $a = 0.381$ nm and $c = 0.353$ nm[2] or a tetragonal structure with $a = b = 0.537$ nm, $c = 0.708$ nm.[3] It has been also shown that the martensitic transformation in the Fe_2MnGa alloys is accompanied with significant changes in their mechanical, magnetic, and transport properties.[1,2,5]

Consequently, one may infer that Fe_2MnGa alloys show an unusually rich metastable behavior for a relatively small deviation from the stoichiometric composition: they may exhibit a BCC structure (defined as a disordered $L2_1$ structure), a FCC structure (*i.e.*, a disordered $L1_2$ structure), or they may exhibit a martensitic transformation from a BCC parent phase to a tetragonal structure defined as a tetragonally distorted BCC structure for a certain range of compositions. In this paper, we report the results of magnetic and transport measurements of Fe_2MnGa alloys with distinct structural orderings and make a comprehensive analysis on how various types of structural orders affect their magnetic and transport properties.

EXPERIMENTAL DETAILS

Several bulk polycrystalline Fe_2MnGa alloys near the stoichiometry 2:1:1 were prepared by melting together pieces of Fe, Mn, and Ga of 99.99% purity in an arc furnace with a water cooled Cu hearth under a 1.3 bar Ar atmosphere. The Ar gas in the furnace before melting was additionally purified by multiple remelting of a $Ti_{50}Zr_{50}$ alloy getter. To promote the volume homogeneity, the ingots were remelted five times. After ingot melting, the weight loss was negligible. The actual alloy compositions were evaluated by using energy dispersive x-ray spectroscopy (see Table I).

Reuse of AIP Publishing content is subject to the terms at: https://publishing.aip.org/authors/rights-and-permissions. Download to IP: 79.191.72.235 On: Sat, 04 Jun 2016 17:02:58

TABLE I. Composition of Fe_2MnGa alloys, amounts of FCC and BCC phases, valence electron concentration, resistivity of alloys at $T = 300$ K, and saturation magnetization measured at $T = 4.2$ K.

Sample No.	Alloy composition (at. %)	FCC phase amount (vol. %)	BCC phase amount (vol. %)	Valence electron concentration (electron/atom)	ρ(300 K) $\times 10^{-6}$ (Ω cm)	Saturation magnetization (emu/g)
1	$Fe_{49}Mn_{25}Ga_{26}$	100	0	6.45	290	120
2	$Fe_{50}Mn_{24}Ga_{26}$	92	8	6.46	257	109
3	$Fe_{50}Mn_{23}Ga_{27}$	71	29	6.42	152	46
4	$Fe_{50}Mn_{22}Ga_{28}$	39	61	6.38	242	61
5	$Fe_{46}Mn_{24}Ga_{30}$	19	81	6.27	550	78
6	$Fe_{52}Mn_{18}Ga_{30}$	0	100	6.32	356	53

The structural characterization of the sample was carried out at room temperature (RT) employing x-ray diffraction (XRD) in $\theta - 2\theta$ geometry with Cu-K_α radiation ($\lambda = 0.15406$ nm). An SC 404 F1 Pegasus differential scanning calorimeter (DSC) was used to determine the phase transformation temperatures. The magnetic properties of the bulk Fe_2MnGa alloy samples were investigated over the temperature range $80 \le T \le 825$ K by measuring the DC-magnetic susceptibility in a weak magnetic field of 5 Oe and by measuring the alloy magnetization over the temperature range $2 \le T \le 400$ K and a range of magnetic fields $0 \le H \le 50$ kOe by using the PPMS-P7000 system. The transport properties of the Fe_2MnGa alloy samples were measured by using the four-probe technique over the range of temperatures $80 \le T \le 600$ K. The samples for the transport measurements, about $1 \times 1 \times 15$ mm^3 in size, were cut from an ingot by using the spark-erosion technique.

Electronic structure calculations (density of states $N(E)$ (DOS), total electron energy, and magnetic properties) of the stoichiometric Fe_2MnGa HA for ordered $L2_1$- (225 space group) and $L1_2$- (123 space group) types of structure (see Fig. 1) as well as for FM and ferrimagnetic (FI) types of magnetic order were calculated by using the WIEN2k code[16] utilizing a full-potential linearized-augmented-plane-wave method.[17] For the exchange-correlation functional, the generalized-gradient-approximation version of Perdew *et al.*[18] was used. Self-consistency was obtained using 816 k-points in the irreducible Brillouin zone. The lattice parameters of the $L2_1$ and $L1_2$ structures obtained as the result of volume optimization were used for the calculations. Additionally, the electronic structure of a tetragonally distorted $L2_1$-phase of Fe_2MnGa alloy was also calculated. The experimental lattice constants for the tetragonal phase[3] were used for the calculations.

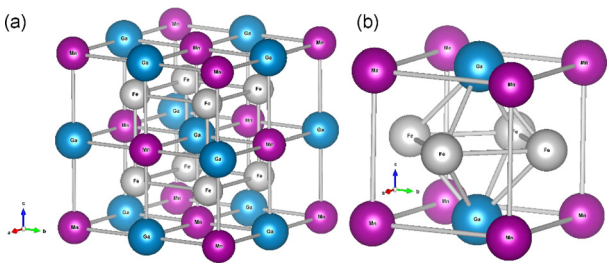

FIG. 1. $L2_1$ (a) and $L1_2$ (b) structures of Fe_2MnGa alloy. The atoms are coded as follows. Fe: gray, Mn: magenta, Ga: blue.

RESULTS AND DISCUSSION

Electronic structure

Our previous results have shown that the $L2_1$ crystalline structure in Fe_2MnGa alloy is stable only for FI type of magnetic ordering.[19] We have found no solution for the FM ordering in the $L2_1$ structure. On the other hand, for the $L1_2$ crystalline structure of a Fe_2MnGa alloy, both the FM and FI types of magnetic order have been shown to be equally probable.

The calculated DOS of a stoichiometric Fe_2MnGa alloy with tetragonal, $L2_1$-, and $L1_2$ types of atomic order shown in Fig. 2 shows that symmetry significantly affects the

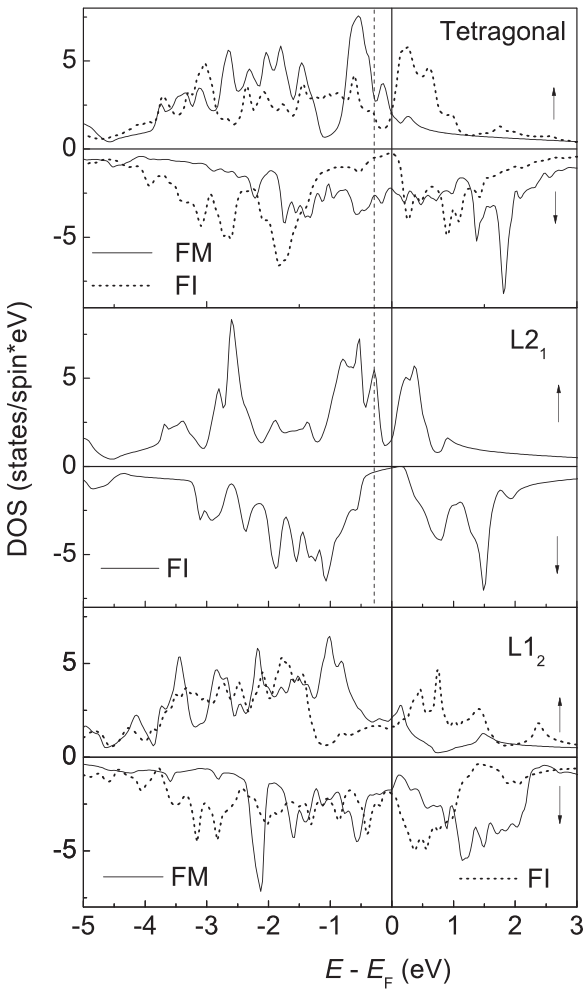

FIG. 2. Density of states of stoichiometric Fe_2MnGa alloy calculated for different types of structural and magnetic order.

Reuse of AIP Publishing content is subject to the terms at: https://publishing.aip.org/authors/rights-and-permissions. Download to IP: 79.191.72.235 On: Sat, 04 Jun 2016 17:02:58

TABLE II. Calculated total and partial magnetic moments per formula unit, DOS at E_F, and total electron energies of Fe_2MnGa alloys with different types of atomic and magnetic orders. Calculated lattice constants are shown together with experimental results.

Structure	Magnetic order	μ_{tot} μ_B	μ_{Fe} μ_B	μ_{Mn} μ_B	μ_{Ga} μ_B	$N(E_F)$ (states/eV spin)	E_{tot} (eV)	a_{calc} nm	a_{exp} nm
Tetragonal	FM	6.355	2.231	2.101	−0.112	5.10	−11296.7456		$a=b=0.5368$, $c=0.7081$
Tetragonal	FI	0.201	−1.620	3.070	0.020	2.43	−11296.7621		$a=b=0.5368$, $c=0.7081$
$L2_1$	FI	2.010	−0.450	2.870	0.000	1.65	−11296.7502	0.5700	0.5871
$L1_2$	FM	6.130	1.980	2.290	−0.090	3.84	−11296.7666	0.3644	0.3701
$L1_2$	FI	0.480	−1.760	2.950	0.002	3.56	−11296.7424	0.3666	

electronic structure of the alloy. In particular, strong differences are observed near the Fermi level E_F. It should also be noted that the spin-up and spin-down states for all types of structure are strongly polarized, since the separate peaks of the up- and down-states neither coincide with energy nor with intensity (see Fig. 2). The main contribution to the DOS is made by the Fe and Mn atoms, whose states are strongly hybridized, as the most intense DOS peaks are formed by the Fe and Mn states coinciding in the energy scale. The Ga contribution to the total DOS is small, i.e., the Ga atoms basically form ionic bonds with the surrounding atoms.

The phase stability of Ni-, Co-, and Fe-based HA has been studied by Entel and Zayak.[14,15] According to them, unstable HA has an intense $N(E)$ peak at E_F, which is responsible for the nesting topology of the Fermi surface and the covalent bonding features. This affects the optical vibrational TA_2 modes of Ni-based system (unlike those based on Co or Fe).[14,15] From this point of view, the stoichometric Fe_2MnGa alloy with $L2_1$ structure and FI magnetic order is stable.[14,15]

Considering the obtained values of $N(E_F)$ and E_{tot} for the different types of atomic and magnetic orders in stoichiometric Fe_2MnGa alloy (see Table II), it is hard to deduce its phase stability. Among the calculated structures, the FI ordered $L2_1$ phase of Fe_2MnGa alloy has the lowest $N(E_F)$, but its E_{tot} is in the middle. The FM $L1_2$ phase of Fe_2MnGa has the lowest E_{tot} but its $N(E_F)$ is nearly twice as big as that for the FI $L2_1$ phase. For these possible types of atomic and magnetic orders of stoichiometric perfectly ordered Fe_2MnGa alloy, $\Delta E_{tot} = 0.0164$ eV (or 190 K). For the tetragonal phase of Fe_2MnGa alloy, the FI magnetic order is more preferable than the FM.

As can be seen in Table II, the main contribution to the total magnetic moment μ_{tot} for the cubic phases of Fe_2MnGa is by moments localized at the Mn. For the tetragonal phase, the magnetic moments localized at Fe and Mn sites give nearly the same contribution to μ_{tot}. The moment localized at Ga is negligible.

Structure

Figure 3 shows the XRD experimental patterns of our samples (open circles). The solid (red) lines through the circles are the results of a Ritveld refinement with the differences between the data and refinement shown in the bottom panels for each sample. According to the XRD data for the Fe_2MnGa alloys, the three furthest samples 1 (2) and 6 have the disordered $L1_2$ (i.e., FCC) and disordered $L2_1$ (i.e., BCC or A2) types of structures, respectively. The fundamental diffraction peaks for these types of structure are shown by two stick diagrams at the top and bottom panels. In a closer examination of the refinements for samples 1 and 2, it is hard to see whether the pure FCC structure obtains for sample 1 or 2. It seems that sample 1 has the less intensive peak (220) from the BCC phase. However, sample 2 has no (400) peak of $L2_1$, which is seen for sample 1. Therefore, it is possible that sample 2 is more homogeneous. Other samples contain both FCC and BCC phases in different ratios (see Fig. 3 and Table I). The amounts of the FCC and BCC phases in the alloys have been evaluated by the ratios of the most intense (111) [for the FCC phase] and (220) [for the BCC phase] diffraction peaks. The samples in Table I and in most of the figures were arranged by the content of the FCC and BCC

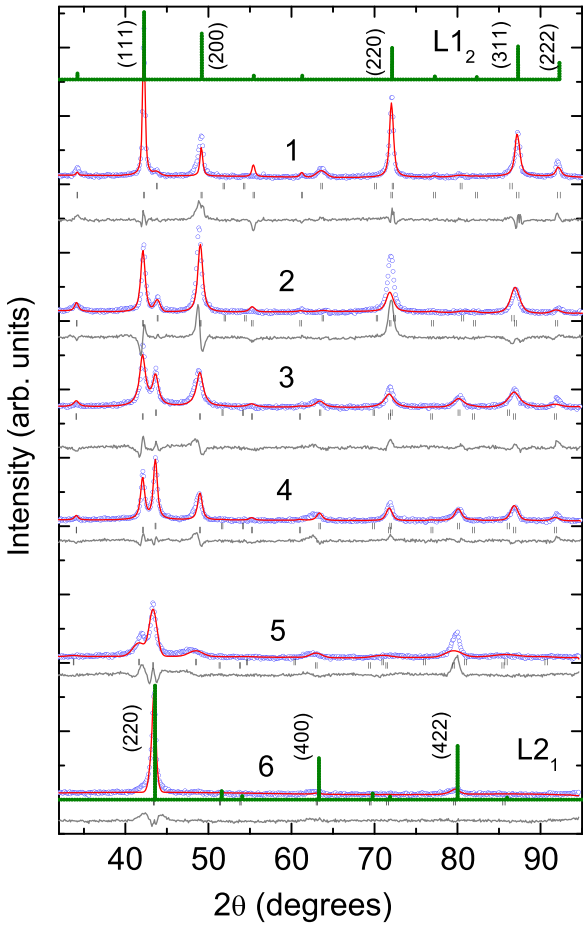

FIG. 3. Experimental (symbols) and simulated (lines) XRD spectra of Fe_2MnGa alloys. Numbers indicate Fe_2MnGa alloy samples. Stick diagrams (green) show the main XRD lines of the $L2_1$ and $L1_2$ structures.

Reuse of AIP Publishing content is subject to the terms at: https://publishing.aip.org/authors/rights-and-permissions. Download to IP: 79.191.72.235 On: Sat, 04 Jun 2016 17:02:58

phases, with some uncertainty concerning samples 1 and 2. It is characteristic that the XRD pattern of sample 5 has significantly broader reflections than that of the other samples. As will be discussed in the Discussion section, such an XRD pattern may be related to a tetragonally distorted BCC structure of a martensitic phase. The experimental values of the lattice constants for the FCC and BCC phases in Fe_2MnGa alloys are close to those found from the first-principles calculations (see Table II).

It is seen that the close probabilities of formation of FI $L2_1$- and FM $L1_2$ phases result in a structural instability of the Fe_2MnGa alloys: An insignificant deviation in the alloy composition from the stoichiometric one results in a change in its phase content. It may be assumed that an increase in Ga content in alloys leads to an increasing probability of the formation of the BCC phase (see Table I).

Figure 4 shows the DSC results of the Fe_2MnGa samples with the regions of interest (A, B, and C) depicted by yellow areas. A large number of not well specified endo- and exo-thermic transformations in the Fe_2MnGa alloys in a temperature range of 400–1100 K can be interpreted as an apparent sign of structural instability of the Fe_2MnGa alloys. In the temperature region "A," one exo- and one endothermic peak are related to the onset of the FCC phase in agreement with Ref. 12. As is shown by the blue dashed lines through 1 and 2, the endothermic peak definitely related to a FCC phase disappears. In contrast, an endothermic peak at about 850 K intensifies and serves as a sign of the onset of a BCC phase. At lower temperatures (region "B"), weak endothermic peaks at 700–800 K are related to a FM/PM transformation. As will be discussed in Fig. 5, the endothermic peaks are the most pronounced for samples 1 and 2 and disappear completely for samples 5 and 6. Eventually, at the lowest temperature range 400–600 K (region "C"), there are some signs (see the discussion of Fig. 5) of a transition attributed to an AFM/FM transformation in the FCC phase. As is depicted by dashed red lines, samples 1 and 2 can be regarded as mostly constituted by the FCC phase with a small admixture of the BCC phase, while samples 5 and 6 are mostly made up of the BCC phase. We conclude that the DSC results are in agreement with the XRD data.

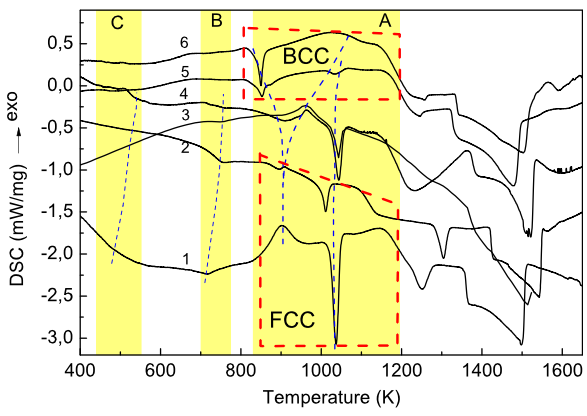

FIG. 4. Differential thermal analysis of bulk Fe_2MnGa alloys. Numbers indicate the alloy samples. Yellow areas depict regions of interest.

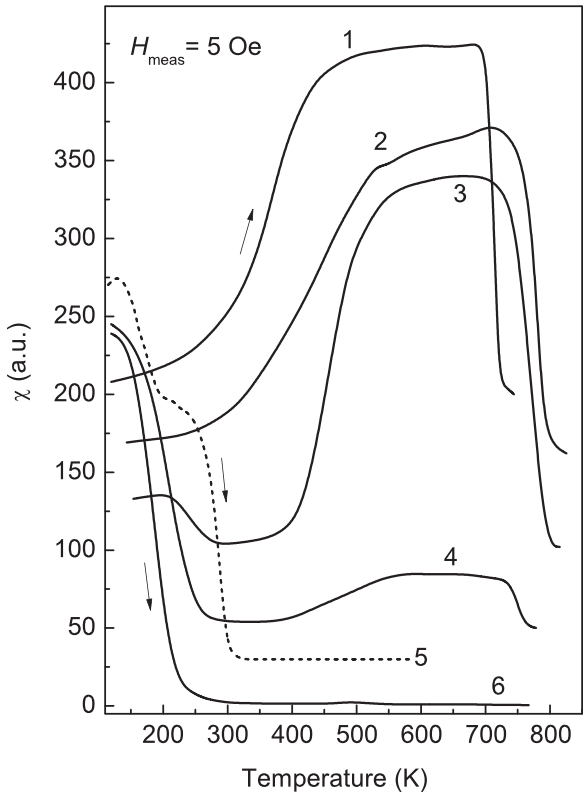

FIG. 5. Temperature dependencies of DC magnetic susceptibility of Fe_2MnGa alloys obtained on warming. The $\chi(T)$ curves of Fe_2MnGa alloys are shifted. Numbers indicate the samples.

Magnetic properties

As shown in Fig. 5, the FCC and BCC phases in the Fe_2MnGa alloys have distinct magnetic properties, which may be determined from the temperature dependencies of the magnetic susceptibility $\chi(T)$ on warming. While the BCC phase (sample 6) is ferromagnetic below its Curie temperature $T_C \approx 200-220$ K, the FCC phase (samples 1 and 2) is ferromagnetic below $T_C \approx 730-750$ K but its susceptibility decreases rapidly below $T \approx 400$ K. The apparently mixed-phase Fe_2MnGa alloys (samples 3 and 4, for example) have $\chi(T)$ being a combination of the temperature dependencies of susceptibilities of the pure BCC and FCC phases. Similar results have already been obtained (Ref. 12), however, with distinct T_C of 400 K for the FCC phase. In contrast, $\chi(T)$ of sample 5 shows an additional drop on warming at about 260 K.

At higher fields of 50–500 Oe, the temperature dependencies of the magnetization shown in Fig. 6 are more complex. In particular, for samples 4 and 6, a long "tail" is seen at $T > 250$ K both on cooling and warming, while the magnetization of sample 5 reveals a clear hysteretic behavior on cooling and warming.

In contrast, for a Fe_2MnGa alloy containing mainly the FCC phase (samples 1 and 2), the magnetization increases with temperature. Sample 3 contains ≈30% of the BCC phase, and its $M(T)$ dependence exhibits the features typical for a mixture of the BCC and FCC phases. It should be emphasized here that $M(T)$ for field cooling and field warming plots for the aforementioned samples do not show any hysteretic behavior.

Reuse of AIP Publishing content is subject to the terms at: https://publishing.aip.org/authors/rights-and-permissions. Download to IP: 79.191.72.235 On: Sat, 04 Jun 2016 17:02:58

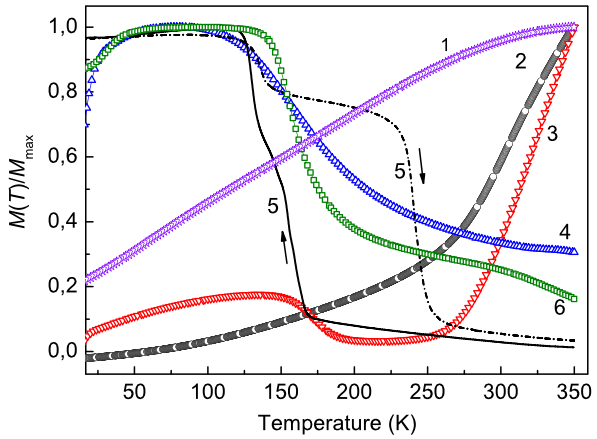

FIG. 6. Temperature dependencies of normalized magnetization of bulk Fe_2MnGa alloys taken at low ($H = 50 \div 500$ Oe) magnetic fields. $M(T)/M_{max}$ plots for all the samples (except sample 5) practically coincide for the cooling and warming scans, only the warming scans are presented. Numbers near the $M(T)/M_{max}$ curves indicate alloy samples.

These unusual temperature dependencies of DC magnetic susceptibility (Fig. 5) and magnetization of Fe_2MnGa alloys containing the FCC-phase taken at relatively weak measuring magnetic fields (Fig. 6) have been observed earlier and explained as resulting from a metamagnetic transformation from low-temperature AFM to a high-temperature FM state.[6–9] At the same time, Passamani *et al.*[11] have explained the temperature dependence of the magnetization of the FCC Fe_2MnGa alloys by different temperature dependencies of magnetization for antiparallel aligned magnetic moments localized at the Fe and Mn sublattices.

A hysteretic behavior of the temperature dependence of the magnetization of sample 5 needs some explanation. In agreement with earlier observations, such an anomaly in $M(T)$ can be definitely ascribed to a martensitic transformation.[1,5] The martensitic transformation is confirmed by independent differential calorimetric measurements. As is seen in Fig. 7, DSC measurements for sample 5 demonstrate clear exothermic and endothermic peaks on cooling and warming, in agreement with the hysteretic behavior of magnetization shown in Fig. 6 for sample 5. Specifically, the temperatures

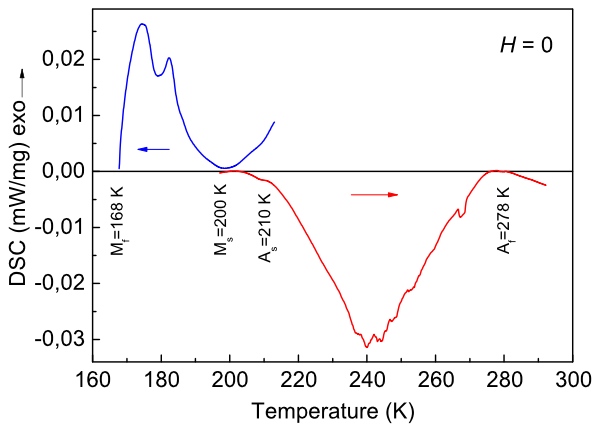

FIG. 7. DSC curves of bulk Fe_2MnGa alloy, sample 5. Ms (As) and Mf (Af) are the start and finish temperatures of martensite M (austenite A), respectively.

of martensite (austenite) start Ms (As) and finish Ms (Af) temperatures determined using DSC (see Fig. 7) are in rough agreement with those that can be evaluated from the magnetization measurements shown in Fig. 6 for sample 5. In contrast, there is no sign of such hysteretic behavior for the other Fe_2MnGa samples (not shown).

As can be seen in Fig. 8, at the still higher magnetic field of 50 kOe, there is a total disappearance of the AFM (or FI) order in the FCC phase. Hence, the $M(T)$ plot for sample 2 reveals a typical dependence of the FM ordering with a rather high Curie temperature of $T_C = 800$ K according to the $\chi(T)$ data shown in Fig. 5. On the other hand, the alloys containing mainly the BCC phase (samples 4 and 6) with metamagnetic behavior show significant magnetization much above their Curie temperatures due to the suppression of spin fluctuations by a high magnetic field. In contrast, the $M(T)$ dependence for sample 5 taken at $H = 50$ kOe significantly differs and exhibits the hysteretic behavior characteristic of a martensitic transformation. This is further confirmed by a shift of 20 K for the forward and reverse martensitic transformation temperatures due to a magnetic field in comparison to those determined by DSC (see Fig. 7). In accordance with the magnetization measurements carried out at low magnetic fields (see Fig. 6), the magnetization at $H = 50$ kOe is 20 emu/g at $T > 300$ K, i.e., much lower than M for the alloys containing the BCC or FCC phases.

Transport properties

Table I shows that the RT values of the resistivity ρ are rather high, perhaps due to both a high resistivity of HA[5] and additional defects caused by the sample preparation. Spark-erosion is known to cause significant distortions of the sample surface to a depth of about 150 μm.[20] Thus, a distorted portion of a specimen with cross section 1×1 mm^2 occupies about 40% of its volume. Therefore, the values of the resistivity Fe_2MnGa alloys should be treated with caution. Nevertheless, in all the investigated Fe_2MnGa alloys, the high resistivity correlates with that found in the literature.[1,5]

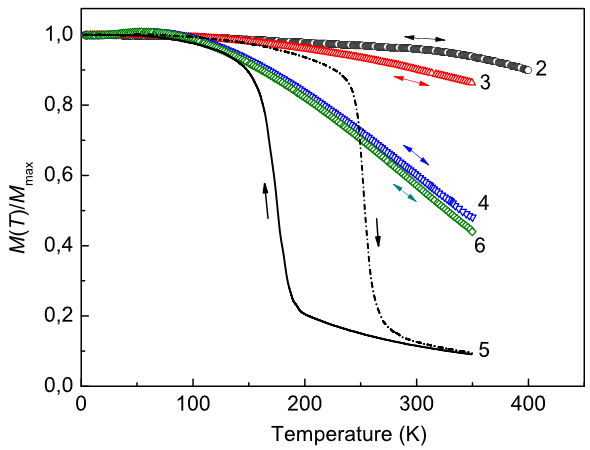

FIG. 8. Temperature dependencies of normalized magnetization of bulk Fe_2MnGa alloys taken at $H = 50$ kOe. Numbers near the $M(T)/M_{max}$ curves indicate alloy sample. The $M(T)/M_{max}$ plots for all the samples (except sample 5) practically coincide for the cooling and warming scans, therefore only the warming scans are presented.

Reuse of AIP Publishing content is subject to the terms at: https://publishing.aip.org/authors/rights-and-permissions. Download to IP: 79.191.72.235 On: Sat, 04 Jun 2016 17:02:58

As shown in Fig. 9, the amounts of each phase (FCC, BCC) in a Fe_2MnGa alloy significantly affect the temperature behavior of the resistivity. Sample 1, containing mostly the FCC phase, shows typically metallic behavior: ρ increases nearly linearly with temperature in a temperature range of 80–550 K. An increase in the amount of the BCC phase (samples 2 and 3) results in saturation of the resistivity at a high temperature range. The visible upturn in the $\rho(T)$ for sample 4 takes place at $T \approx 400$ K, where the metallic behavior of the resistivity with a positive temperature coefficient of resistivity (TCR) gives way to a semiconductor-like one with a negative TCR. The temperature dependence of the resistivity for a Fe_2MnGa alloy containing mainly the BCC phase (sample 6) exhibits a clear "cusp" at which the TCR changes its sign. This temperature is close to its Curie temperature. A similarly striking change in the character of electron transport as the system undergoes the transition from ferromagnetic to paramagnetic has been found in Fe_2MnSi and Co_2TiSn HAs.[21–23]

Unlike the apparent similarity with other samples (e.g., samples 4 and 6) both in structure and the phase amount, the transport properties of sample 5 are different. Thus, the resistivity value of sample 5 exhibits (on warming) a rapid and significant increase of about 30% at $T \approx 250$ K, where the TCR changes its sign. Furthermore, only the $Fe_{46}Mn_{24}Ga_{30}$ alloy (sample 5) has a significant temperature hysteresis of resistivity on heating and cooling (see the inset in Fig. 9). Comparing the obtained experimental $\rho(T)$ dependence of sample 5 with the results in the literature, the nature of the peculiarity at $T \approx 250$ K can be definitely ascribed to a reverse martensitic transformation.[1,5]

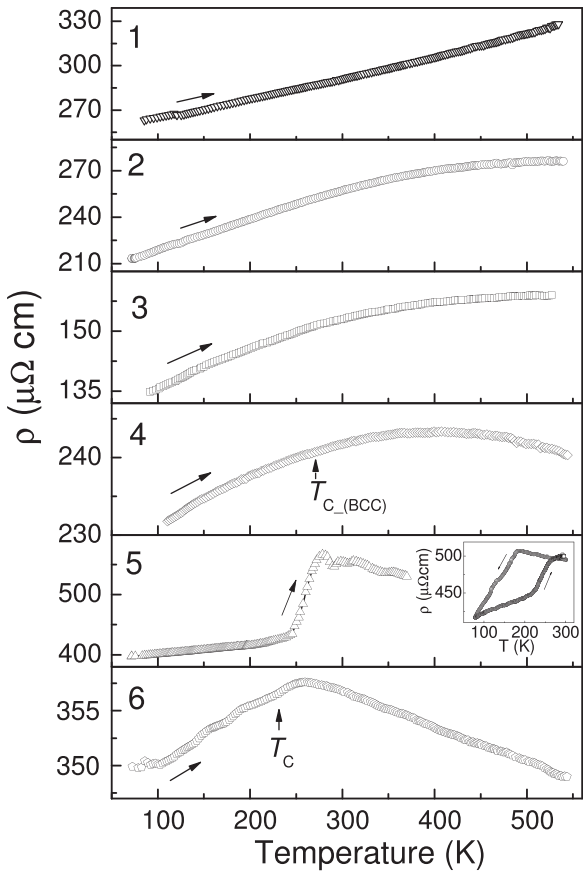

FIG. 9. Resistivity vs. temperature of the Fe_2MnGa alloys. Numbers on the panels indicate sample number. Inset in the plot for sample 5 shows a hysteretic behavior of $\rho(T)$ for another sample with the same composition as sample 5.

DISCUSSION

The structural characterization of these Fe_2MnGa alloys (see Fig. 3) and the first-principles calculations (see Table I) suggest that a relatively small deviation from the stoichiometric composition in $Fe_{50}Mn_{25}Ga_{25}$ with the FCC structure lead to the emergence of the BCC phase. The BCC phase is ferromagnetic at $T < 220$ K. In contrast, the FCC phase is ferromagnetic at high temperatures ($T_C \approx 730$ K) and at $T < 300$ K becomes ferri- or anti-ferromagnetic. However, this ferri-/anti-ferromagnetic ordering is unstable, and at high magnetic fields of 50 kOe, it experiences a metamagnetic transformation to a ferromagnetic ordering. Additionally, the structural instability of the Fe_2MnGa alloys results in a tetragonal distortion of the BCC phase: it becomes energetically more stable in some circumstances due to a martensitic transformation. The martensitic transformation in sample 5 is confirmed by the magnetic (Figs. 6 and 8), DSC (Fig. 7), and partially by the transport (Fig. 10) measurements. A more precise analysis of the XRD data for sample 5 suggests that the occurrence of a tetragonal phase is possible even though the austenite finish temperature Af is at 278 K, i.e., slightly below the RT.

A closer review of the XRD spectra for samples 4, 5, and 6 shows that the diffraction peak of sample 5 located at $2\Theta = 48.2°$ is slightly shifted to the small-angle region in comparison with the (200) reflection for the FCC phase for the other samples. According to Zhu *et al.*[1] and Omori *et al.*,[3] the martensite phase has noticeably different lattice parameters ($a = b = 0.5328$ nm, $c = 0.7113$ nm for $Fe_{50.0}Mn_{22.5}Ga_{27.5}$ alloy or $a = b = 0.5368$ nm, $c = 0.7081$ nm for $Fe_{44}Mn_{28}Ga_{28}$ alloy) from that of the parent austenite BCC phase ($a = 0.5826$ nm or $a = 0.5864$ nm). The modeling of the XRD spectrum for tetragonal phase by using the experimental data obtained by Omori *et al.*[3] reveals that the experimental diffraction peaks located at $2\Theta = 42.2$ and 48.2° can be nicely fitted with the (202) and (220) reflections in the model XRD spectrum. The presence of the (004), (400), (224), and (422)

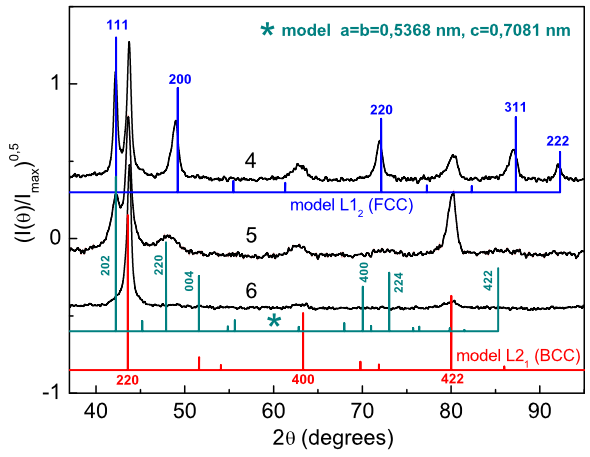

FIG. 10. Experimental XRD spectra of mainly BCC-phase containing Fe_2MnGa alloys together with those for $L1_2$, $L2_1$, and tetragonally distorted $L2_1$ lattices.

Reuse of AIP Publishing content is subject to the terms at: https://publishing.aip.org/authors/rights-and-permissions. Download to IP: 79.191.72.235 On: Sat, 04 Jun 2016 17:02:58

reflections related to the tetragonal phase can also be further confirmed by comparison of the experimental XRD spectrum with the simulated one. Other intense peaks in the experimental spectrum for sample 5 (e.g., the peaks at $2\Theta = 43.8$, 62.8, and 80.1°) are definitely formed by the (220), (400), and (422) reflections of the BCC phase. However, the (111) and (200) reflections from the FCC phase may also contribute to the resulting intensity of the reflections at $2\Theta = 42.2$ and 48.2°. Therefore, our analysis of the RT XRD pattern of sample 5 suggests that it contains some traces of the tetragonal phase in the BCC matrix. The amount of the tetragonal phase at RT in the sample 5 evaluated using experimental XRD data is close to 20%.

The question now arises as to how the martensitic transformation happens in Fe_2MnGa alloys for a valence electron concentration e/a below 6.4 (or 6.3 according to our measurements). The complex dependence of the presence of a martensitic transformation on the composition is often approximated by (e/a).[14] However, the universality of this approach is not clear.[14,15] Nevertheless, it is worth noting that, among Fe_2MnGa alloys, a martensitic transformation has been observed earlier exclusively for alloys containing the BCC phase.[1–5] Stoichiometric Fe_2MnGa alloy has $e/a = 6.5$ electrons/atom. It is seen (see Table I) that an increase in the BCC phase content in Fe_2MnGa alloys is accompanied by a decrease in e/a. The only Fe_2MnGa alloy with the martensitic transformation has the lowest $e/a = 6.27$. On the other hand, a martensitic transformation for Fe_2MnGa has been previously observed for $6.27 < e/a < 6.40$.[1–5]

It is supposed that the martensitic transformation in Ni-based HA is due to a structural instability driven by their peculiar electron band structure, specifically, due to the formation of an intense $N(E)$ peak at E_F.[14,15] For example, in Ni_2MnGa with a BCC structure, the Fermi level E_F lies in a valley of antibonding minority-spin $3d$ states, which leads to a structural instability.[14] This instability can be lifted by transforming to a tetragonal structure because of a gap formed in the minority-spin states around E_F. A closer look at the density of states shown in Fig. 2 for Fe_2MnGa with the $L2_1$ ($e/a = 6.5$) and the tetragonal structure (FM or FI) reveals a similar behavior for majority-spin DOS. Assuming that e/a is now 6.22, the Fermi level would be 0.3 eV lower than that for $e/a = 6.5$ and would lie in the DOS peak—clearly an unstable state. Therefore, similarly to what is observed in Ni_2MnGa, the instability would be lifted by transforming to a tetragonal structure with the pseudo-gap at E_F depicted by a dashed line in Fig. 2. Such a scenario would explain why sample 5 with $e/a = 6.27$ exhibits a martensitic transformation.

Bearing in mind that our samples contain both BCC and FCC phases and reveal metamagnetism at low temperatures (for the FCC phase), it is shown in Fig. 11 that there is some correlation between e/a and the magnetic moment per formula unit at RT. In Fig. 11, the black circles depict the experimental values of the magnetic moment. The gray circles depict values taken from the literature.[1,3,5,8,11] The dashed red line is a guide to the eye and shows, for low values of e/a, the magnetization between 0 μ_B/f.u. of the paramagnetic BCC phase and 2 μ_B/f.u. for the $L2_1$ (FI) structure. For

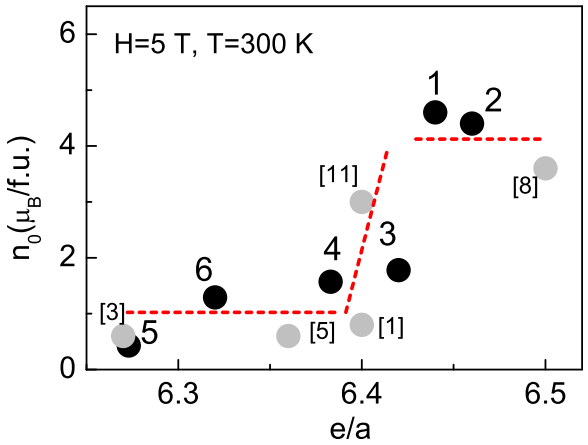

FIG. 11. Magnetization (in μ_B per formula unit) vs. the valence electron concentration e/a of the investigated Fe_2MnGa alloys (black circles and numbers) and the results taken from the literature (gray circles with reference numbers. The red dashed line is a guide to the eye.

the highest values of e/a, the magnetization is lower than 6 μ_B/f.u. for the FCC $L1_2$ phase. It is seen that the magnetization seems to show a jump at e/a of 6.4, but the other processing parameters also play a role,[12] so that samples 4 and 6 do not exhibit any martensitic transformation and have the notably higher magnetization of 1.5 μ_B/f.u. at RT. The magnetic properties of sample 5 differ from those of the other investigated Fe_2MnGa alloys not only in a significant hysteresis on warming and cooling but also in having the lowest magnetization value of 0.5 μ_B/f.u. at $T > 300$ K obtained either at low or high magnetic fields (see Figs. 6 and 8). In contrast, in the martensite phase, the magnetization is 3.8 μ_B/f.u. in agreement with the earlier experiments.[2] Such a strange behavior, i.e., transformation from a nearly paramagnetic parent BCC phase to a strongly ferromagnetic tetragonal martensite phase, is the opposite to that of the most known Ni-Mn-based shape memory alloys.[10,24] Therefore, in contrast to a fragile magnetism of the BCC phase in Fe_2MnGa alloys, the magnetism of the tetragonal phase is very stable, in agreement with first-principles calculations (see Table II).

It has been shown that a change in FCC to BCC amounts in Fe_2MnGa alloys causes the gradual changes in $\rho(T)$ dependencies from the metallic-like to the semiconductor-like behavior (see Fig. 10). The martensitic transformation observed in sample 5 supplements this tendency by a rapid increase in resistivity in a narrow temperature range (see Fig. 10). The resistivity described within a simple relaxation time τ approximation in a nearly free electron model (see, for example, Ref. 25) reads as

$$\rho = \frac{m^*}{e^2 \tau n_{\text{eff}}} = \frac{3}{e^2 \tau v^2} \frac{1}{N(E_{\text{F}})}, \tag{1}$$

where m^* and n_{eff} are the effective mass and the effective density of conduction electrons per unit volume, respectively; v and $N(E_F)$ are the velocity and the DOS at the Fermi energy. According to results of the first-principles calculations (see Table II and Fig. 2), the value of $N(E_F)$ for the tetragonal phase is nearly five times higher than that for the $L2_1$ phase. Thus, the experimentally observed decrease in

Reuse of AIP Publishing content is subject to the terms at: https://publishing.aip.org/authors/rights-and-permissions. Download to IP: 79.191.72.235 On: Sat, 04 Jun 2016 17:02:58

resistivity upon transformation from austenite to martensite can be explained by a significant increase in $N(E_F)$ for the tetragonal phase. The values of $N(E_F)$ for the $L1_2$ phase with FM or FI types of magnetic order are more than three times larger than that for the $L2_1$ phase. This also correlates with the experimentally observed dependencies of $\rho(T)$ of those Fe_2MnGa alloys that exhibit a martensitic transformation.

Several mechanisms of charge carrier scattering have been suggested to explain the temperature dependence of the resistivity of metals. Electron–phonon, electron–electron, and electron–magnon (spin-disorder) scattering make major contributions to the resulting temperature dependence of ferromagnetic metals with positive TCR. Thus, for example, electron–phonon based scattering ($\sim T$ for $T \gg \Theta_D$) can be described by the Bloch–Grüneisen function and its modifications.[26] Electron–electron scattering is proportional to $\sim T^2$.[27] Electron–magnon (spin-disorder) scattering mechanisms are proportional to $\sim T^{\alpha}$, where $\frac{3}{2} < \alpha < T^{\frac{9}{2}}$.[28] Electron–magnon (spin-disorder) scattering usually reaches its maximum near the Curie temperature; above T_C, the spin-disorder mechanism is independent of T. Therefore, for some ferromagnetic metals and alloys (including ferromagnetic HA[23]), a distinct change in the slope of the $\rho(T)$ dependence can be expected above T_C.[29–31]

The Ioffe–Regel criterion predicts the conditions when the resistivity is saturated with temperature: when the mean free path l of the electrons is of the interatomic distance d

$$\rho^{\text{I–R}} = 55 \times \frac{d}{r_B}(\mu\Omega\text{cm}), \tag{2}$$

where d is the nearest interatomic distance and $r_B = 0.0529$ nm is the Bohr radius.[32] For the FCC and BCC phases of Fe_2MnGa alloys, d is 0.262 and 0.254 nm, respectively. Thus, $\rho^{\text{I–R}}$ for Fe_2MnGa alloys should be 272 $\div$ 264 $\mu\Omega$ cm. The experimentally determined values of the alloy resistivity are close to these parameters. However, unlike the expected change of the slope in $\rho(T)$ at T_C or even its saturation above T_C, for the high-resistive Fe_2MnGa HA (samples 4, 6), a negative slope of $\rho(T)$ at high temperatures is also observed in Fig. 9. A similar behavior of $\rho(T)$ at $T > T_C$ has also been observed for the other HAs.[21–23,31]

There are several reasons for the appearance of the negative TCR in metals. The negative TCR of some transition metal alloys is usually attributed to the strong atomic scattering's leading to a weak localization or variable-range-hopping.[33,34] Mooij[35] has suggested an empirical rule for such alloys: the TCR is negative if the resistivity of the alloy exceeds $\rho_{\text{alloy}} > 150\ \mu\Omega$ cm. The temperature dependence of the resistivity of sample 6 with the BCC structure shows a nearly linear decrease with temperature above T_C (Fig. 9). The quantum interference effects such as weak localization and electron–electron interactions give rise to a rather high value of ρ and a negative TCR in disordered systems.[33] Furthermore, the variable-range-hopping conductivity[34] can also lead to a negative TCR. In the variable-range-hopping mechanism proposed by Mott,[34] electrons preferentially hop to the localized states that are close in energy but not necessarily close spatially, and the conductivity is

$$\frac{1}{\rho(T)} = \sigma(T) = \sigma_0 \exp\left[-\left(\frac{T_0}{T}\right)^p\right], \tag{3}$$

where $p = 1/4$. The weak localization mechanism shows that the conductivity depends on the temperature

$$\Delta\sigma = \alpha(2e^2/\pi^2\hbar)\ln T, \tag{4}$$

where the coefficient α is negative.[33]

As shown in Fig. 12, the temperature dependence of the conductivity of sample 6, containing mostly the BCC phase, changes at T_C of 240 K (i.e., $\ln(240) = 5.48$) in accordance with the weak localization mechanism. However, it is worth noting that the variable-range-hopping mechanism also gives a reasonable approximation to the experimental data (not shown).

Among the investigated Fe_2MnGa alloys, sample 4 also contains a significant amount of BCC phase (about 60%) with a Curie temperature of 250 K. However, no peculiarity near T_C can be seen. This is most probably due to a bridging by a lower resistivity FCC phase. For Fe_2MnGa alloys rich in the FCC phase (samples 1–3), the metamagnetic transformation from AFM (or FI) to FM takes place at $T \approx 300 \div 350$ K (on warming, see Fig. 3). However, there is no peculiarity in $\rho(T)$ in this range of temperatures. Thus, for these high-resistive Fe_2MnGa alloys, spin-disorder scattering makes a negligible contribution in comparison with the other scattering mechanisms.

SUMMARY

The experimental results for Fe_2MnGa alloys shown in this paper supplement those previously obtained, as resulting from their metastable behavior. There are some important points aiming at an explanation of the variety of magnetic and electronic transport properties of Fe_2MnGa alloys.

(1) The first-principles calculations for the stoichiometric Fe_2MnGa alloy with different types of atomic and magnetic orders show that the $L2_1$ structures with the ferrimagnetic ordering as well as the $L1_2$ structure with the ferromagnetic ordering are the most stable structures. In contrast, the tetragonally distorted $L2_1$ phase with any

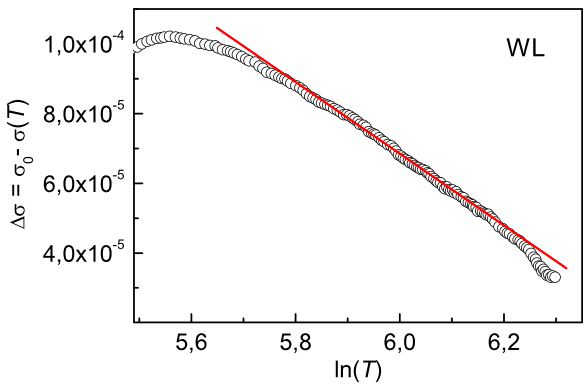

FIG. 12. Change of the electrical conductivity vs. $\ln(T)$ of a Fe_2MnGa alloy containing mostly the BCC phase (sample 6) for $T > T_C$. Red continuous line shows a fit according to Eq. (4) for a weak localization mechanism.

Reuse of AIP Publishing content is subject to the terms at: https://publishing.aip.org/authors/rights-and-permissions. Download to IP: 79.191.72.235 On: Sat, 04 Jun 2016 17:02:58

type of magnetic order is less probable for the stoichiometric Fe_2MnGa alloy.

(2) Several single or two-phase off-stoichiometric Fe_2MnGa alloys have been investigated with $6.25 < e/a < 6.5$.

(3) It has been shown that Fe_2MnGa alloys with nearly pure BCC or FCC phases have distinct magnetic properties, with FM–PM and AFM–FM–PM transformations, respectively. The Fe_2MnGa alloys with mixed BCC and FCC phases have the features typical for both BCC and FCC phases.

(4) The transport properties of the Fe_2MnGa alloys containing FCC and BCC phases correlate with the results of first-principles calculations of these phases. The negative TCR of a Fe_2MnGa alloy containing a pure BCC phase can be explained by a weak-localization mechanism.

(5) We have found that the $Fe_{46}Mn_{24}Ga_{30}$ alloy with the lowest value of valence electron concentration ($e/a = 6.27$) contains predominantly the BCC phase and has a martensitic transformation with $M_s = 168$ K and $A_s = 225$ K for $H = 0$ as well as $M_s = 193$ K and $A_s = 237$ K for $H = 50$ kOe. The transformation is accompanied with significant changes in its magnetic and transport properties. The martensite phase is in a FM state, while the parent phase is in a PM state.

ACKNOWLEDGMENTS

This work has been supported by the project "Marie Skłodowska-Curie Research and Innovation Staff Exchange (RISE)" Contract No. 644348 with the European Commission, as part of the Horizon2020 Programme.

The authors are deeply appreciative of the help of A. V. Terukov and M. S. Nizameev in the XRD and DSC measurements.

[1]W. Zhu, E. K. Liu, L. Feng, X. D. Tang, J. L. Chen, G. H. Wu, H. Y. Liu, F. B. Meng, and H. Z. Luo, Appl. Phys. Lett. **95**, 222512 (2009).
[2]T. Omori, K. Watanabe, R. Y. Umetsu, R. Kainuma, and K. Ishida, Appl. Phys. Lett. **95**, 082508 (2009).
[3]T. Omori, K. Watanabe, X. Xu, R. Umetsu, R. Kainuma, and K. Ishida, Scr. Mater. **64**, 669 (2011).
[4]C. A. Jenkins, A. Scholl, R. Kainuma, H. J. Elmers, and T. Omori, Appl. Phys. Lett. **100**, 032401 (2012).
[5]V. V. Khovaylo, T. Omori, K. Endo, X. Xu, R. Kainuma, A. P. Kazakov, V. N. Prudnikov, E. A. Ganshina, A. I. Novikov, Y. O. Mikhailovsky, D. E. Mettus, and A. B. Granovsky, Phys. Rev. B **87**, 174410 (2013).
[6]X. D. Tang, W. H. Wang, W. Zhu, E. K. Liu, G. H. Wu, F. B. Meng, H. Y. Liu, and H. Z. Luo, Appl. Phys. Lett. **97**, 242513 (2010).
[7]X. D. Tang, W. H. Wang, G. H. Wu, F. B. Meng, H. Y. Liu, and H. Z. Luo, Appl. Phys. Lett. **99**, 222506 (2011).
[8]T. Gasi, A. K. Nayak, M. Nicklas, and C. Felser, J. Appl. Phys. **113**, 17E301 (2013).
[9]C. Shih, X. Zhao, H. Chang, W. Chang, and Z. Zhang, J. Alloys Compd. **570**, 14 (2013).
[10]A. N. Vasilev, A. D. Bozhko, V. V. Khovailo, I. E. Dikshtein, V. G. Shavrov, V. D. Buchelnikov, M. Matsumoto, S. Suzuki, T. Takagi, and J. Tani, Phys. Rev. B **59**, 1113 (1999).
[11]E. Passamani, C. Larica, G. Viali, J. Andrez, A. Takeuchi, V. Nascimento, V. Rodriguez, C. Rojas-Ayala, and E. Baggio-Saitovitch, J. Alloys Compd. **628**, 164 (2015).
[12]H. Okumura, E. Hashiba, and K. Nagata, Intermetallics **49**, 65 (2014).
[13]M. Yin, P. Nash, and S. Chen, Intermetallics **57**, 34 (2015).
[14]P. Entel, V. D. Buchelnikov, V. V. Khovailo, A. T. Zayak, W. A. Adeagbo, M. E. Gruner, H. C. Herper, and E. F. Wassermann, J. Phys. D: Appl. Phys. **39**, 865 (2006).
[15]A. T. Zayak, P. Entel, K. M. Rabe, W. A. Adeagbo, and M. Acet, Phys. Rev. B **72**, 054113 (2005).
[16]P. Blaha, K. Schwarz, G. K. H. Madsen, D. Kvasnicka, and J. Luitz, *WIEN2k, An Augmented Plane Wave+Local Orbitals Program for Calculating Crystal Properties* (Techn. Universit Aat Wien, Wien, Austria, 2001).
[17]E. Wimmer, H. Krakauer, M. Weinert, and A. J. Freeman, Phys. Rev. B **24**, 864 (1981).
[18]J. P. Perdew, K. Burke, and M. Ernzerhof, Phys. Rev. Lett. **77**, 3865 (1996).
[19]Y. V. Kudryavtsev, N. V. Uvarov, V. N. Iermolenko, I. N. Glavatskyy, and J. Dubowik, Acta Mater. **60**, 4780 (2012).
[20]V. F. Mazanko, D. S. Gerzriken, V. M. Mironov, D. V. Mironov, and S. A. Bobyr (Naukova Dumka, Kiev, Ukraine, 2014) (in Russian).
[21]N. I. Kourov, A. V. Korolev, V. V. Marchenkov, A. V. Lukoyanov, and K. A. Belozerova, Phys. Solid State **55**, 977 (2013).
[22]N. I. Kourov, V. V. Marchenkov, A. V. Korolev, L. A. Stashkova, S. M. Emelyanova, and H. W. Weber, Phys. Solid State **57**, 700 (2015).
[23]S. Majumdar, M. K. Chattopadhyay, V. K. Sharma, K. J. S. Sokhey, S. B. Roy, and P. Chaddah, Phys. Rev. B **72**, 012417 (2005).
[24]T. Krenke, M. Acet, E. F. Wassermann, X. Moya, L. Mañosa, and A. Planes, Phys. Rev. B **72**, 014412 (2005).
[25]J. S. Dugdale, *The Electrical Properties of Disordered Metals* (Cambridge University Press, 1995).
[26]B. L. Altshuler, Zh. Eksp. Teor. Fiz. [Sov. Phys. JETP] **75**, 1330 (1978).
[27]B. Loegel and F. Gautie, J. Phys. Chem. Solids **32**, 2723 (1971).
[28]D. L. Mills, A. Fert, and I. A. Cambell, Phys. Rev. B **4**, 196 (1971).
[29]S. Bose, J. Kudrnovsky, and V. Drchal, World J. Eng. **9**, 13 (2012).
[30]J. Kudrnovsky, V. Drchal, I. Turek, S. Khmelevskyi, J. K. Glasbrenner, and K. D. Belashchenko, EPJ Web Conf. **40**, 12001 (2013).
[31]J. Barth, G. H. Fecher, B. Balke, S. Ouardi, T. Graf, C. Felser, A. Shkabko, A. Weidenkaff, P. Klaer, H. J. Elmers, H. Yoshikawa, S. Ueda, and K. Kobayashi, Phys. Rev. B **81**, 064404 (2010).
[32]O. Gunnarsson, M. Calandra, and J. E. Han, Rev. Mod. Phys. **75**, 1085 (2003).
[33]P. W. Anderson, E. Abrahams, and T. V. Ramakrishnan, Phys. Rev. Lett. **43**, 718 (1979).
[34]N. F. Mott, J. Non-Cryst. Solids **1**, 1 (1968).
[35]J. H. Mooij, Phys. Status Solidi A **17**, 521 (1973).

Reuse of AIP Publishing content is subject to the terms at: https://publishing.aip.org/authors/rights-and-permissions. Download to IP: 79.191.72.235 On: Sat, 04 Jun 2016 17:02:58